RSC Advances

This is an *Accepted Manuscript*, which has been through the Royal Society of Chemistry peer review process and has been accepted for publication.

Accepted Manuscripts are published online shortly after acceptance, before technical editing, formatting and proof reading. Using this free service, authors can make their results available to the community, in citable form, before we publish the edited article. This *Accepted Manuscript* will be replaced by the edited, formatted and paginated article as soon as this is available.

You can find more information about *Accepted Manuscripts* in the **Information for Authors**.

Please note that technical editing may introduce minor changes to the text and/or graphics, which may alter content. The journal's standard **Terms & Conditions** and the **Ethical guidelines** still apply. In no event shall the Royal Society of Chemistry be held responsible for any errors or omissions in this *Accepted Manuscript* or any consequences arising from the use of any information it contains.

Journal Name

PAPER

Green and size-controllable synthesis of photoluminescent carbon nanoparticles from waste plastic bags

Yaoping Hu,[a] Jing Yang,[a,b] Jiangwei Tian,[a] Li Jia,[a] and Jun-Sheng Yu*[a]

We have developed a facile approach for green and size-controllable synthesis of photoluminescent carbon nanoparticles (CNPs) by hydrothermal treatment of various waste plastic bags (WPBs) in low-concentration H_2O_2 solutions (≤5.0 wt%). This approach requires none of toxic regents, severe synthetic conditions, or complicated procedures. Fine control over the particle size of the CNPs is achieved by
10 simply changing the H_2O_2 concentration, and the higher H_2O_2 concentration leads to the smaller particle size of the CNPs. An interesting formation mechanism of the CNPs derived from WPBs has been proposed including thermo-oxidative degradation, polymerization, carbonization, and passivation. It is found that the CNPs can selectively quantify the concentration of Fe^{3+} from 10 to 400 μM with a detection limit as low as 2.8 μM. Moreover, the strong photoluminescence, excellent optical stability, low
15 cytotoxicity, and good water-dispersibility of the CNPs make them suitable candidates for cellular imaging. The simple method developed here presents a new way for effective reuse of WPBs and realizes the encouraging "waste-to-treasure" conversion.

Introduction

Tremendous efforts have been made on the synthesis of
20 photoluminescent carbon nanoparticles (CNPs) in recent years due to their unique properties[1,2] and potential applications in bioimaging,[3-5] drug delivery,[6] sensors,[7-11] optoelectronics,[12,13] and photocatalysis.[14-16] Since the pioneering work on the preparation of fluorescent CNPs from single-walled carbon nanotubes,[17]
25 various precursors, including graphite,[18,19] graphene,[13,16,20] multiwalled carbon nanotube,[21] fullerene,[22,23] small organic molecules,[24-33] biomasses,[34-40] soot,[41-43] and so on, have been employed as carbon sources for fabricating CNPs. Among these precursors, the waste materials, for instance soot, towards CNPs
30 are preferable in terms of significantly reducing production cost and considerably saving resources. Unfortunately, concentrated strong acids such as highly corrosive sulfuric acid and nitric acid are usually required in the reaction process of the CNPs made from soot,[41-43] which raises the environmental concerns and limits
35 their further applications. Thus far, low-cost production of waste-derived CNPs with eco-friendly methods is still a great challenge.

The increasing production of waste plastic bags (WPBs) has a profound negative impact on our environment and society. Recently, despite numerous countries have introduced legislation
40 restricting the sale of plastic bags in a bid to reduce littering, it is still estimated that between 500 billion and 1 trillion plastic bags are used and million tons of plastic bags are discarded each year worldwide.[44] WPBs create visual pollution and have harmful effects on aquatic and terrestrial animals.[45] They are resistant to
45 degradation and last for hundreds of years to fully break down.[46] Proper disposal of WPBs in environment-benign routes or

chemical conversion of WPBs into valuable materials remains an outstanding problem.

Herein, we demonstrate the first use of WPBs as a carbon
50 source for facile synthesis of fluorescent CNPs in low-concentration H_2O_2 solutions (≤5.0 wt%) through thermo-oxidative degradation, polymerization, carbonization, and passivation. In comparison to the previous synthetic methods, our approach is truly green, as only H_2O_2, an ideal and waste-
55 avoiding oxidant, is demanded in the reaction. The approach is also universal and practical, since various WPBs with different compositions obtained from dustbins are feasible for producing CNPs. It is noticeable that fine control over the particle size of the CNPs is achieved by simply changing the H_2O_2 concentration,
60 and the higher H_2O_2 concentration leads to the smaller particle size of the CNPs. The resultant CNPs are functionalized with abundant oxygenous groups and exhibit satisfactory photoluminescence quantum yield, excellent optical stability, low cytotoxicity, and good water-dispersibility. Such CNPs can serve
65 as effective fluorescent probes for label-free, sensitive, and selective detection of Fe^{3+} with a detection limit as low as 2.8 μM. Moreover, the CNPs have provided successful application for cellular imaging.

Experimental

Reagents and materials

All the WPBs were obtained from the dustbins. Hydrogen peroxide (30 wt%) was purchased from Nanjing Chemical Reagents Factory (Nanjing, China). 3-(4,5-Dime-thylthiazol-2-yl)-2,5-diphenyltetrazolium bromide (MTT) was purchased from

Sigma Chemical Co. (St. Louis, MO, USA). The water used in the experiments was purified through a Millipore water purification system. All other reagents and chemicals were of analytical grade and used without further purification.

Synthesis of CNPs

CNPs were prepared by hydrothermal treatment of WPBs in H_2O_2 solution. In a typical synthesis, WPBs were cut into small pieces. Then, 0.2 g of the plastic fragments was put into a 50 mL Teflon-lined stainless-steel autoclave containing 30 mL of H_2O_2 solution in a certain concentration (0.0, 0.2, 1.0, 2.0, 3.0, and 5.0 wt%). After hydrothermal treatment at 180 °C for 12 h, the autoclave cooled down naturally. The resulting solution was centrifuged at 12000 rpm for 10 min to remove the residue. Further purification of CNPs was conducted through a dialysis tube (molecular weight cut off: 1000 Da) for 3 days in the dark (changed deionized water every 8 h). The power of CNPs was obtained by freeze-drying the purified solution. The final productions of CNPs were 2.4, 15.1, 65.3, 101.8, 89.7, and 75.2 mg, respectively from 0.0, 0.2, 1.0, 2.0, 3.0, and 5.0 wt% H_2O_2 solutions.

Fluorescence Assay of Fe^{3+}

In a typical run, 6 mg of CNPs was dissolved in 100 mL of a pH 7.0 PBS (20 mM) buffer solution. Then, 0.1 mL of a certain concentration of Fe^{3+} ions was added into 0.9 mL of the CNPs dispersion. The fluorescence emission spectra with excitation wavelength of 320 nm were recorded after reaction for 10 min. The sensitivity and selectivity measurements were conducted in triplicate.

Cellular toxicity test

The cytotoxicity test of CNPs was carried out using MTT assay on Hela cells. Hela cells were first seeded to 96-well plates at a seeding density of 1×10^4 cells per well in 200 μL medium, which was incubated at 37 °C for 24 h. After rinsing with PBS, Hela cells were incubated with 200 μL culture medium containing serial concentrations of CNPs for 48 h. Afterward, the medium was removed and the cells were washed with PBS. Then, 20 μL of 5 mg mL^{-1} MTT solution was added to each cell well. The 96-well plates were further incubated for 4 h, followed by removing the culture medium with MTT, and then 200 μL of DMSO was added. The optical density of the mixtures at 490 nm was measured. Cell viability was expressed as percentage of absorbance relative to control. The control was obtained in the absence of CNPs.

Cellular imaging

Hela cells were seeded in each well of a Confocal Dish (Coverglass-Bottom Dish) and cultured at 37 °C for 24 h. Then, the cells were incubated with CNPs at a final concentration of 100 μg mL^{-1} for 1 h. After that, the cells were washed thoroughly three times with PBS. The cellular images were taken by a confocal laser scanning microscope (Leica TCS SP5) and the emission was measured over the range of 450-600 nm with excitation at 405 nm.

Instruments and measurements

Elemental analysis of the WPBs was achieved using an Elemental

Vario MiCRO analyzer. Transmission electron microscopy (TEM) images and selected-area electron-diffraction (SAED) patterns were taken on a JEM-2100 microscope operating at an accelerated voltage of 200 kV. Power X-ray diffraction (XRD) measurement was performed with a Shimadu XRD-6000 powder X-ray diffractometer with Cu Ká radiation (1.54178 Å). X-ray photoelectron spectroscopy (XPS) measurements were carried out with a PHI 5000 VersaProbe X-ray photoelectron spectrometer. Fourier transformed infrared (FTIR) spectrum was collected in the KBr medium on a Nicolet 6700 FTIR spectrometer. The ^{13}C-NMR spectrum was recorded on a Bruker Avance 400 MHz spectrometer. Zeta potential was measured on a nano Z zeta potential analyzer. Ultraviolet-visible (UV-vis) absorption spectrum was taken on a Shimadzu UV-3600 spectrophotometer. Photoluminescence (PL) spectra were acquired on a RF-5301PC spectrophotometer. Fluorescence lifetime was monitored using an Edinburgh FLS 920 time-resolved spectroscope.

Results and discussion

A green synthetic strategy

The vast majority of WPBs are made from polyethylene, while a small amount of WPBs are composed of polypropylene, polyvinyl chloride, or polyvinylidene chloride. All these raw materials of WPBs are chemically stable polymers, which are resistant to dilute strong acids and gentle oxidants under ambient conditions. In order to greenly convert the "inert" WPBs into fluorescent CNPs which contain oxygenic groups, we designed a H_2O_2-assisted hydrothermal synthetic strategy. Hydrothermal technique was employed because it can provide an excellent reaction environment (temperature above 100 °C and pressure above 1 bar) for preparation of nanomaterials. H_2O_2 was selected as an environmentally benign oxidant and oxygen feedstock. The typical advantage of H_2O_2 is that it changes into water without poison residue after releasing oxygen.

Waste fruit-carrying plastic bags obtained from dustbins containing C 69.86 wt% and H 11.51 wt% (elemental analysis) were used in the first case for the synthesis of CNPs (The photograph of the WPBs is given in Fig. S1). Fig. 1 shows the products of WPBs which were heated in different concentrations of H_2O_2 (from 0.0 to 5.0 wt%) at 180 °C for 12 h and the centrifuged solutions of CNPs. It is obvious that the reaction

Fig. 1 (a) The products of WPBs which were heated in different concentrations of H_2O_2 (from left to right: 0.0, 0.2, 1.0, 2.0, 3.0, and 5.0 wt%) at 180 °C for 12 h, and (b) the centrifuged solutions of CNPs.
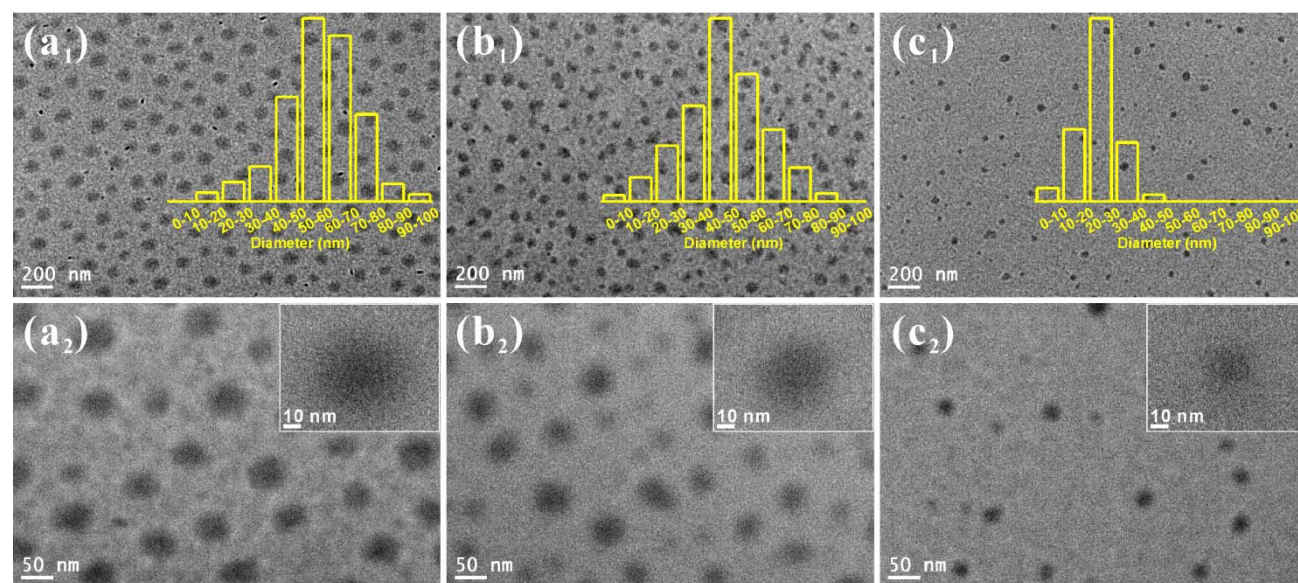
Fig. 2 TEM images of CNPs-1 (a_1, a_2), CNPs-2 (b_1, b_2), and CNPs-3 (c_1, c_2). The statistical size distributions of CNPs-1 (a_1, inset), CNPs-2 (b_1, inset), and CNPs-3 (c_1, inset). HRTEM images of CNPs-1 (a_2, inset), CNPs-2 (b_2, inset), and CNPs-3 (c_2, inset).

conducted in pure water (0.0 wt% H_2O_2) resulted in a colorless solution and bulk residue. When the concentration of H_2O_2 increased from 0.0 to 2.0 wt%, the colour of the solution turned from colorless to light yellow to red brown, and the residue became smaller in size. These results indicate that both the oxidation degree of WPBs and the yield of CNPs increased. However, if the concentration of H_2O_2 further raised from 2.0 to 5.0 wt%, the solution of CNPs conversely changed from red brown to light yellow. Additionally, many bubbles generated in the autoclave as the concentration of H_2O_2 reached 5.0 wt% (Fig. S2). We proposed that too high concentration of H_2O_2 leaded to over-oxidation of WPBs, producing the gas of CO_2 which was associated with the bubbles and reducing the yield of CNPs. To confirm the proposal, we weighted the CNPs and found that the CNPs synthesized in 2.0 wt% H_2O_2 solution got the maximum yield of 51 wt%, whereas that prepared in higher or lower concentration of H_2O_2 solution had lower production yield (Fig. S3). We tried to synthesize CNPs at different temperatures (120, 140, 160 °C) and found that no CNPs formed for the temperature below 140 °C. As the temperature increased to 160 °C, CNPs generated (Fig. S4). However, the yield of the CNPs was just 42 wt%, lower than that synthesized at 180 °C. Thus, the temperature of 180 °C was selected.

Size control, structure, and composition of the CNPs

By varying the concentration of H_2O_2, we have realized the size-controllable synthesis of monodisperse CNPs. For the sake of succinctness, the samples fabricated in 0.2, 2.0, and 5.0 wt% H_2O_2 are respectively named CNPs-1, CNPs-2, and CNPs-3. TEM images (Fig. 2) show that the CNPs are nearly spherical and uniform in size. The statistical size distributions of CNPs-1 (Fig. 2a_1, inset), CNPs-2 (Fig. 2b_1, inset), and CNPs-3 (Fig. 2c_1, inset) are 10-100 nm, 0-90 nm, and 0-50 nm, with maximum populations at 50-60 nm, 40-50 nm, and 20-30 nm (200 random nanoparticles were accounted in each case). The result reveals that the average diameter of the CNPs can be well controlled by

tuning the concentration of H_2O_2, and the higher concentration of H_2O_2 renders the smaller particle size of the CNPs. The high-resolution TEM (HRTEM) images (Fig. 2a_2, b_2 and c_2, insets) show that the diffraction contrasts of the CNPs are very low and no clear lattice fringes are found, which are suggestive of their amorphous nature.[40] The XRD patterns of the CNPs (Fig. S5) exhibits broad peaks at 20.96-21.28°, corresponding to a graphite structure. The calculated interlayer spacing of the CNPs ranges from 0.417 to 0.423 nm, larger than that of natural graphite (0.335 nm), which is attribute to the existence of functional groups on the edges of the CNPs.[26]

XPS was used to analyze the chemical composition of the CNPs. All the survey spectra (Fig. 3a) exhibit two prominent features of C_{1s} and O_{1s}. The content of each element is displayed in Fig. 3a. It is calculated that the atomic ratio of O_{1s}/C_{1s} is 0.361, 0.415, and 0.497 respectively for CNPs-1, CNPs-2, and CNPs-3. Reasonably, the CNPs synthesized in higher H_2O_2 concentration exhibit higher atomic ratio of O_{1s}/C_{1s}. The C_{1s} spectra (Fig. 3b) can be deconvoluted into three peaks, corresponding to C-C/C=C at 284.3 eV, C-O at 286.5 eV, and C=O at 288.0 eV.[35] Their relative contents are listed in Table 1 based on the calculations of the integral areas. The increasing content of C=O from 12.31% to 19.19%, and to 25.04% for CNPs-1, CNPs-2, and CNPs-3 reveals the increasing oxidation degree of the nanoparticles. The FTIR spectrum (Fig. 4a) presents the absorption bands of O-H at 3413 cm^{-1}, C=O at 1712 cm^{-1}, C=C at 1575 cm^{-1}, C-O at 1177 cm^{-1}, and C-H at 2939, 2859, 1414, and 1380 cm^{-1}. ^{13}C NMR spectroscopy is a power technique to investigate different kinds of carbons within the CNPs. The ^{13}C NMR spectrum (Fig. 4b) shows abundant C-C aliphatic carbons in 0-90 ppm (including C-O carbons in 40-90 ppm), a small amount of C=C alkene/aromatic carbons in 134 and 166 ppm, and a number of C=O carboxylic/carbonyl carbons in 180-220 ppm.[47] These findings agree well with the XPS and FTIR analysis. The CNPs possess negative Zeta potentials (Fig. S6) due to carboxylic groups on the surface. All the observations indicate that the CNPs

have been functionalized with plentiful oxygen-containing groups, such as hydroxyl, epoxy, carbonyl, and carboxyl, which make them well dispersed in water.
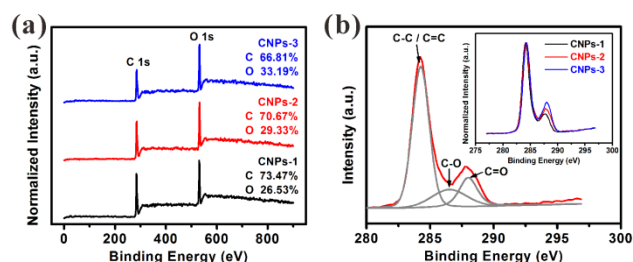

Fig. 3 (a) Normalized XPS survey spectra of CNPs-1, CNPs-2, and CNPs-3. (b) C$_{1s}$ spectrum of CNPs-2. Inset in (b): normalized C$_{1s}$ spectra of CNPs-1, CNPs-2, and CNPs-3.

Table 1 Analysis of C$_{1s}$ spectra of CNPs-1, CNPs-2, and CNPs-3.

Sample	C-C/C=C (%)^a	C-O (%)^a	C=O (%)^a
CNPs-1	73.01	14.68	12.31
CNPs-2	66.37	14.44	19.19
CNPs-3	62.95	12.00	25.04

^{a} The relative contents are based on the calculations of the integral areas.
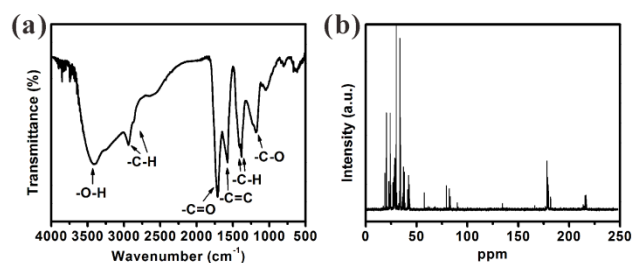
Fig. 4 (a) FTIR spectrum and (b) ^{13}C NMR spectrum of CNPs-2.

Formation mechanism of the CNPs

Based on the structural details described on the above section, we proposed a potential formation mechanism of the CNPs derived from WPBs. The CNPs formation is suggested to proceed *via* four stages, including thermo-oxidative degradation, polymerization, carbonization, and passivation (Fig. 5). In the initial stage, thermal oxidation of the WPBs took place in the presence of H$_2$O$_2$, and the polyethylene chain of the WPBs was cut into small oxidized species that contain hydroxyl, carbonyl, carboxyl, *etc*. Then, the oxidized species assembled through hydrogen bonding and polymerized into soluble polymers by intermolecular dehydration or aldol condensation, which leads to a short single burst of nucleation.[48] After that, carbonization of the polymers occurred by intramolecular dehydration. In this stage, sp^2 C=C bonds and even aromatic rings generated, bringing
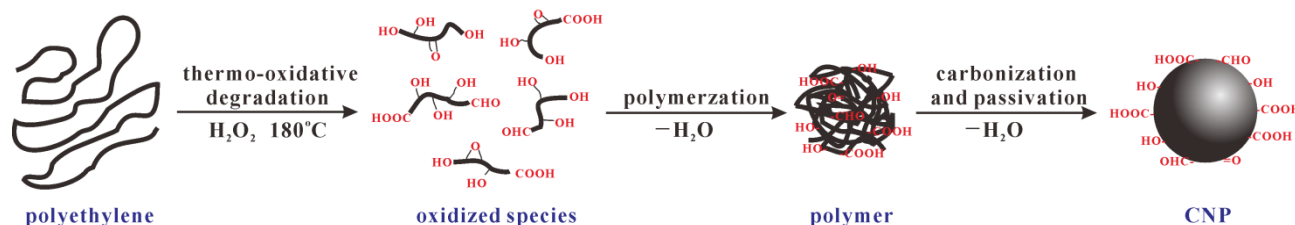
about hydrophobic carbon cores. At the same time, the remained oxidized species in the solution diffused to the particle surfaces, resulting in particle growth and hydrophilic surface passivation.[49,50] Thus, the oxygen-functionalized CNPs formed. To confirm the proposed formation mechanism, time-dependent FTIR spectra were carried out (Fig. S7). The FTIR spectrum of WPBs shows intense absorption bands of C-H at 2924, 2850, and 1463 cm^{-1}, indicating the presence of abundant aliphatic hydrocarbon. After hydrothermal treatment in 2.0 wt% H$_2$O$_2$ solution at 180 °C for 1 h, a part of WPBs was oxidized and dissolved in water. The FTIR spectrum of the oxidized species exhibits that three new peaks of O-H at 3440 cm^{-1}, C=O at 1645 cm^{-1}, and C-O at 1100 cm^{-1} emerge, and the absorption bands of C-H at 2924, 2850 cm^{-1} become much weaker, which are suggestive of the thermo-oxidative degradation of the WPBs. As the reaction proceeded for 2 h, water-soluble light yellow intermediate products generated. The FTIR spectrum of these intermediate products reveals the characteristic absorption bands of esters: C=O stretching vibration at 1707 cm^{-1}, C-O-C asymmetric stretching vibrations at 1200 and 1178 cm^{-1}, and O-C-O bending vibration at 641 cm^{-1}. The newly generated bands of esters indicate the intermolecular dehydration of the oxidized species, demonstrating that the polymerization is in progress. When the reaction time was prolonged to 5 h, a fresh peak of C=C at 1571 cm^{-1} appeared. Then, the C=C peak became stronger with time. The formed C=C units build up the carbogenic core of the CNPs. This step is so-called carbonization. Therefore, the time-dependent FTIR spectra positively support the proposed formation mechanism. We deduce that the higher H$_2$O$_2$ concentration is in favor of cleaving the polyethylene into shorter oxidized chains, and ultimately producing the CNPs with smaller sizes.

Optical properties of the CNPs

We have studied the optical properties of the CNPs. As shown in the insets of Fig. 6a, the aqueous solution of CNPs-2 in a concentration of 0.7 mg mL^{-1} is pale yellow in daylight, but exhibits a bright blue color with UV light irradiation. It has a featureless UV-vis absorption spectrum (Fig. 6a). The PL spectra of CNPs-2 (Fig. 6b) show the strongest emission peak at 438 nm for excitation at 320 nm. The emission peak gradually shifts from 423 to 485 nm (violet to green) when the excitation wavelength is tuned from 300 to 400 nm. The excitation wavelength dependent PL behavior of CNPs is probably attributed to different particle sizes and diverse surface emissive trap sites.[18] As displayed in Fig. S8, the PL intensity of CNPs-2 remains nearly unchanged when the concentration of NaCl ranges from 0.0 to 1.0 mol L^{-1},

Fig. 5 A proposed formation mechanism of the CNPs derived from the WPBs that are composed of polyethylene.

suggesting their excellent optical stability at different ionic strengths. The CNPs-2 possesses a pH-insensitive photoluminescence within pH 3-8 (Fig. S9). However, the emission peak slightly blue-shifts with PL intensity enhancing as pH further increases from 8 to 11. This phenomenon is related to the deprotonation of the carboxyl groups of the nanoparticles under alkaline condition.[51] The PL decay profile of CNPs-2 (Fig. S10) can be well fitted into a double-exponential decay function with τ_1 of 1.68 ns (31.6%) and τ_2 of 6.43 ns (68.4%), suggesting that two different emissive centres, namely electronic conjugate structures and surface traps, exist.[52] The average PL lifetime is 4.93 ns. The quantum yield of CNPs-2 is determined to be 3.85% by using quinine sulfate (54.6% in 0.1 M sulphuric acid) as a standard, comparable to those of reported values.[39,52] It should be mentioned that despite having different particle sizes, the CNPs-1 and CNPs-3 perform similar optical properties to CNPs-2 (Fig. S11), with quantum yields of 3.36% and 4.08% respectively.
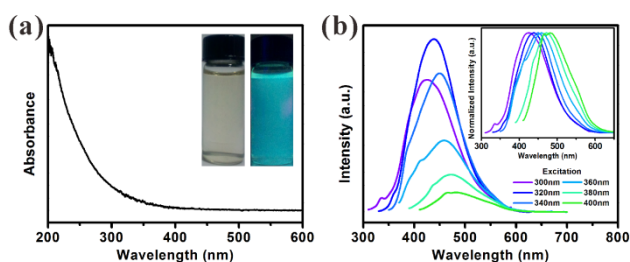

Fig. 6 (a) UV-vis absorption spectrum and (b) PL spectra at different excitation wavelengths of CNPs-2. Inset in (a): photographs of the aqueous solution of CNPs-2 in a concentration of 0.7 mg mL^{-1} under daylight (left) and UV (365 nm) light (right). Inset in (b): normalized PL spectra at different excitation wavelengths of CNPs-2.

CNPs derived from various WPBs

Various WPBs without any classification obtained from dustbins were used as starting materials for green synthesis of photoluminescent CNPs. The elemental analysis (Table S1) shows that the compositions of these WPBs (syringe-packing plastic bag (a), garbage plastic bag (c), soap-packing plastic bag (d), stationery-carrying plastic bag (e), and toilet roll-packing plastic bag (f)) are C 79.05-87.48 wt% and H 12.98-13.80 wt%, except that one (food fresh-keeping plastic bag (b)) contains C 29.62 wt% and H 3.32 wt%. The special one is made of polyvinylidene chloride, while others are constituted by polyethylene or polypropylene. Fig. 7 reveals that despite derived from different WPBs, the CNPs all exhibit broad UV-vis absorptions, and perform excitation wavelength dependent PL behaviors. The quantum yields of the CNPs are 1.18-4.49%, and the production yields of the CNPs are 10.7-52.3% (Table S1). The successful preparation of CNPs from a variety of WPBs strongly demonstrates that our method is universal and practical.

Selective sensing of Fe^{3+}

Fe^{3+} is a biologically important metal ion and plays an essential role in oxygen uptake, oxygen metabolism, and electron transfer.[11,53] We attempted to use the CNPs as fluorescent probes for detection of Fe^{3+}. Fig. 8a records a gradual decrease of PL intensity as Fe^{3+} concentration increases from 0 to 800 μM, revealing that the Fe^{3+} can quench the PL of CNPs. Fig. 8b displays the quenching ratio as a function of Fe^{3+} concentration.
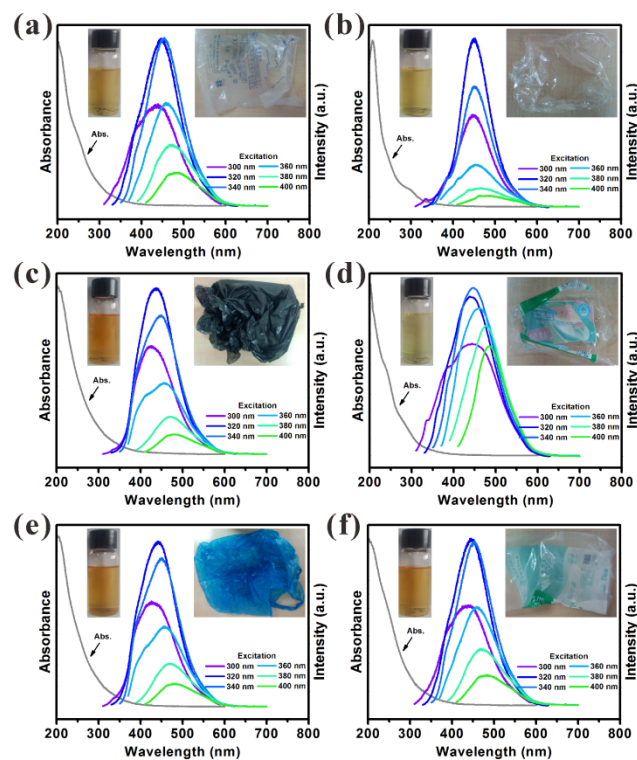

Fig. 7 UV-vis absorption spectra and PL spectra at different excitation wavelengths of CNPs derived from (a) syringe-packing plastic bag, (b) food fresh-keeping plastic bag, (c) garbage plastic bag, (d) soap-packing plastic bag, (e) stationery-carrying plastic bag, and (f) toilet roll-packing plastic bag. Upper left insets: photographs of the aqueous solutions of CNPs derived from different WPBs. Upper right insets: photographs of the different WPBs as the starting materials for synthesis of CNPs. The synthesis was conducted in 2.0 wt% H_2O_2 solution at 180 °C for 12 h.

A nice linear relationship with R^2 of 0.996 is addressed over the concentration range of 10-400 μM. The theoretical detection limit is calculated to be 2.8 μM, lower than the maximum level (0.3 mg L^{-1}, equivalent to 5.4 μM) of Fe^{3+} permitted in drinking water by the U.S. Environmental Protection Agency.[54] The sensing system performs high selectivity toward Fe^{3+}. Other metal ions, including K^+, Ca^{2+}, Co^{2+}, Cu^{2+}, Hg^{2+}, Mg^{2+}, Mn^{2+}, Ni^{2+}, Zn^{2+}, Pb^{2+}, Cd^{2+}, Fe^{2+}, Cr^{3+}, and Al^{3+} at a concentration of 400 μM under the same conditions as those used with Fe^{3+} have minor or negligible PL quenching effects (Fig. S12). Thus, the fluorescent CNPs can be considered as candidate materials for feasible analysis of Fe^{3+} in biological system.
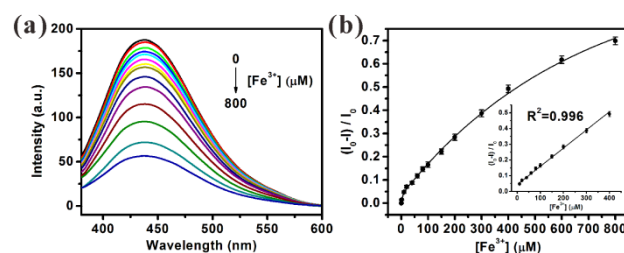

Fig. 8 (a) The PL response of CNPs-2 upon addition of various concentrations of Fe^{3+} in a pH 7.0 solution (from top: 0, 1, 10, 20, 40, 60, 80, 100, 150, 200, 300, 400, 600, and 800 μM). (b) The relationship between $(I_0-I)/I_0$ and concentration of Fe^{3+} from 0 to 800 μM. Inset in (b): a linear region as the concentration of Fe^{3+} ranges from 10 to 400 μM.

Cellular imaging

To assess the fluorescent CNPs for bioimaging application, MTT assay was measured to first evaluate the cytotoxicity of the CNPs. It was found that more than 90% of the Hela cells remained alive even incubated with the CNPs in a concentration of 600 μg mL^{-1} for 48 h (Fig. S13), meaning low cytotoxicity of the CNPs. Fig. 9 show the confocal laser scanning microscopy images of Hela cells which have been treated with the CNPs in a concentration of 100 μg mL^{-1} for 1 h. Since the control experiment has demonstrated the negligible autofluorescence of the Hela cells (Fig. S14), the intense blue fluorescence inside the Hela cells is undoubtedly from the CNPs, which indicates that the CNPs have penetrated the membranes and gotten into the cells in such a short time (1 h). These observations prove that the as-synthesized CNPs can serve as promising fluorescent probes for cellular imaging.
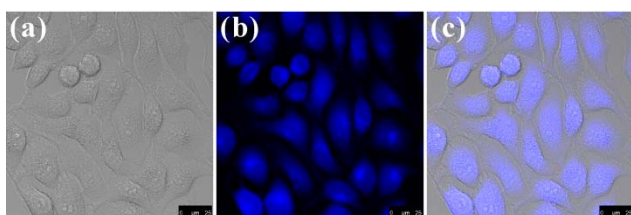

Fig 9 (a) A Bright-field microphotograph of Hela cells. (b) A confocal fluorescence microphotograph of Hela cells incubated with CNPs-2 in a concentration of 100 μg mL^{-1} for 1 h (λ_{ex} = 405 nm). (c) An overlay image of (a) and (b).

Conclusions

In summary, a H$_2$O$_2$-assisted hydrothermal strategy has been developed for the synthesis of photoluminescent CNPs from various WPBs through thermo-oxidative degradation, polymerization, carbonization, and passivation. This strategy is actually green and facile, as it requires none of toxic regents, severe synthetic conditions, or complicated procedures. Noticeably, the particle size of the CNPs can be well controlled by changing the H$_2$O$_2$ concentration, and higher H$_2$O$_2$ concentration is in favor of generating CNPs with smaller particle size. The resulting CNPs have been functionalized with plentiful oxygenic groups and exhibit fascinating optical properties, excellent biocompatibility, low cytotoxicity, and good water-dispersibility. Such CNPs possess highly sensitive and selective recognition of Fe^{3+} ions. In addition, they can serve as promising fluorescent probes for bioimaging. Our study is important for waste management, because it provides a new route to cleanly convert the waste plastic products into valuable carbon nanomaterials.

Acknowledgements

Notes and references

^{a} *State Key Laboratory of Analytical Chemistry for Life Science, School of Chemistry and Chemical Engineering, Nanjing University, Nanjing 210093, P.R. China. Fax: +86(25) 83594957; Tel: +86(25) 83594957; E-mail: jsyu@nju.edu.cn; nju_jsyu@yahoo.com*
^{b} *School of Pharmacy, Nanjing Medical University, Nanjing 210029, P.R. China.*

1   S. N. Baker and G. A. Baker, *Angew. Chem., Int. Ed.*, 2010, **49**, 6726-6744.
2   H. T. Li, Z. H. Kang, Y. Liu and S. T. Lee, *J. Mater. Chem.*, 2012, **22**, 24230-24253.
3   L. Cao, X. Wang, M. J. Meziani, F. S. Lu, H. F. Wang, P. J. G. Luo, Y. Lin, B. A. Harruff, L. M. Veca, D. Murray, S. Y. Xie and Y. P. Sun, *J. Am. Chem. Soc.*, 2007, **129**, 11318-11319.
4   S. T. Yang, L. Cao, P. G. J. Luo, F. S. Lu, X. Wang, H. F. Wang, M. J. Meziani, Y. F. Liu, G. Qi and Y. P. Sun, *J. Am. Chem. Soc.*, 2009, **131**, 11308-11309.
5   P. J. G. Luo, S. Sahu, S. T. Yang, S. K. Sonkar, J. P. Wang, H. F. Wang, G. E. LeCroy, L. Cao and Y. P. Sun, *J. Mater. Chem. B*, 2013, **1**, 2116-2117.
6   J. Tang, B. Kong, H. Wu, M. Xu, Y. C. Wang, Y. L. Wang, D. Y. Zhao and G. F. Zheng, *Adv. Mater.*, 2013, **25**, 6569-6574.
7   L. Zhou, Y. H. Lin, Z. Z. Huang, J. S. Ren and X. G. Qu, *Chem. Commun.*, 2012, **48**, 1147-1149.
8   Q. Qu, A. W. Zhu, X. L. Shao, G. Y. Shi and Y. Tian, *Chem. Commun.*, 2012, **48**, 5473-5475.
9   W. B. Lu, X. Y. Qin, S. Liu, G. H. Chang, Y. W. Zhang, Y. L. Luo, A. M. Asiri, A. O. Al-Youbi and X. P. Sun, *Anal. Chem.*, 2012, **84**, 5351-5357.
10   Y. Q. Dong, G. L. Li, N. N. Zhou, R. X. Wang, Y. W. Chi and G. N. Chen, *Anal. Chem.*, 2012, **84**, 8378-8382.
11   K. G. Qu, J. S. Wang, J. S. Ren and X. G. Qu, *Chem.-Eur. J.*, 2013, **19**, 7243-7249.
12   V. Gupta, N. Chaudhary, R. Srivastava, G. D. Sharma, R. Bhardwaj and S. Chand, *J. Am. Chem. Soc.*, 2011, **133**, 9960-9963.
13   Y. Li, Y. Hu, Y. Zhao, G. Q. Shi, L. E. Deng, Y. B. Hou and L. T. Qu, *Adv. Mater.*, 2011, **23**, 776-780.
14   H. T. Li, X. D. He, Z. H. Kang, H. Huang, Y. Liu, J. L. Liu, S. Y. Lian, C. H. A. Tsang, X. B. Yang and S. T. Lee, *Angew. Chem., Int. Ed.*, 2010, **49**, 4430-4434.
15   L. Cao, S. Sahu, P. Anilkumar, C. E. Bunker, J. A. Xu, K. A. S. Fernando, P. Wang, E. A. Guliants, K. N. Tackett and Y. P. Sun, *J. Am. Chem. Soc.*, 2011, **133**, 4754-4757.
16   S. J. Zhuo, M. W. Shao and S. T. Lee, *ACS Nano*, 2012, **6**, 1059-1064.
17   X. Y. Xu, R. Ray, Y. L. Gu, H. J. Ploehn, L. Gearheart, K. Raker and W. A. Scrivens, *J. Am. Chem. Soc.*, 2004, **126**, 12736-12737.
18   Y. P. Sun, B. Zhou, Y. Lin, W. Wang, K. A. S. Fernando, P. Pathak, M. J. Meziani, B. A. Harruff, X. Wang, H. F. Wang, P. J. G. Luo, H. Yang, M. E. Kose, B. L. Chen, L. M. Veca and S. Y. Xie, *J. Am. Chem. Soc.*, 2006, **128**, 7756-7757.
19   L. Y. Zheng, Y. W. Chi, Y. Q. Dong, J. P. Lin and B. B. Wang, *J. Am. Chem. Soc.*, 2009, **131**, 4564-4565.
20   Y. Li, Y. Zhao, H. H. Cheng, Y. Hu, G. Q. Shi, L. M. Dai and L. T. Qu, *J. Am. Chem. Soc.*, 2012, **134**, 15-18.
21   J. G. Zhou, C. Booker, R. Y. Li, X. T. Zhou, T. K. Sham, X. L. Sun and Z. F. Ding, *J. Am. Chem. Soc.*, 2007, **129**, 744-745.
22   J. Lu, P. S. E. Yeo, C. K. Gan, P. Wu and K. P. Loh, *Nat. Nanotechnol.*, 2011, **6**, 247-252.
23   M. X. Gao, C. F. Liu, Z. L. Wu, Q. L. Zeng, X. X. Yang, W. B. Wu, Y. F. Li and C. Z. Huang, *Chem. Commun.*, 2013, **49**, 8015-8017.
24   H. Zhu, X. L. Wang, Y. L. Li, Z. J. Wang, F. Yang and X. R. Yang, *Chem. Commun.*, 2009, 5118-5120.

RSC Advances Accepted Manuscript

25 H. T. Li, X. D. He, Y. Liu, H. Huang, S. Y. Lian, S. T. Lee and Z. H. Kang, *Carbon*, 2011, **49**, 605-609.

26 L. B. Tang, R. B. Ji, X. K. Cao, J. Y. Lin, H. X. Jiang, X. M. Li, K. S. Teng, C. M. Luk, S. J. Zeng, J. H. Hao and S. P. Lau, *ACS Nano*, 2012, **6**, 5102-5110.

27 J. Jiang, Y. He, S. Y. Li and H. Cui, *Chem. Commun.*, 2012, **48**, 9634-9636.

28 A. B. Bourlinos, A. Stassinopoulos, D. Anglos, R. Zboril, M. Karakassides and E. P. Giannelis, *Small*, 2008, **4**, 455-458.

29 F. Wang, S. P. Pang, L. Wang, Q. Li, M. Kreiter and C. Y. Liu, *Chem. Mater.*, 2010, **22**, 4528-4530.

30 Y. Q. Dong, J. W. Shao, C. Q. Chen, H. Li, R. X. Wang, Y. W. Chi, X. M. Lin and G. N. Chen, *Carbon*, 2012, **50**, 4738-4743.

31 A. B. Bourlinos, R. Zboril, J. Petr, A. Bakandritsos, M. Krysmann and E. P. Giannelis, *Chem. Mater.*, 2012, **24**, 6-8.

32 A. B. Bourlinos, A. Bakandritsos, A. Kouloumpis, D. Gournis, M. Krysmann, E. P. Giannelis, K. Polakova, K. Safarova, K. Hola and R. Zboril, *J. Mater. Chem.*, 2012, **22**, 23327-23330.

33 A. B. Bourlinos, M. A. Karakassides, A. Kouloumpis, D. Gournis, A. Bakandritsos, I. Papagiannouli, P. Aloukos, S. Couris, K. Hola, R. Zboril, M. Krysmann, E. P. Giannelis, *Carbon*, 2013, **61**, 640-643.

34 J. Wang, C. F. Wang and S. Chen, *Angew. Chem., Int. Ed.*, 2012, **51**, 9297-9301.

35 S. Sahu, B. Behera, T. K. Maiti and S. Mohapatra, *Chem. Commun.*, 2012, **48**, 8835-8837.

36 P. C. Hsu, Z. Y. Shih, C. H. Lee and H. T. Chang, *Green Chem.*, 2012, **14**, 917-920.

37 M. J. Krysmann, A. Kelarakis and E. P. Giannelis, *Green Chem.*, 2012, **14**, 3141-3145.

38 S. Liu, J. Q. Tian, L. Wang, Y. W. Zhang, X. Y. Qin, Y. L. Luo, A. M. Asiri, A. O. Al-Youbi and X. P. Sun, *Adv. Mater.*, 2012, **24**, 2037-2041.

39 C. Z. Zhu, J. F. Zhai and S. J. Dong, *Chem. Commun.*, 2012, **48**, 9367-9369.

40 W. Li, Z. H. Zhang, B. A. Kong, S. S. Feng, J. X. Wang, L. Z. Wang, J. P. Yang, F. Zhang, P. Y. Wu and D. Y. Zhao, *Angew. Chem., Int. Ed.*, 2013, **52**, 8151-8155.

41 H. P. Liu, T. Ye and C. D. Mao, *Angew. Chem., Int. Ed.*, 2007, **46**, 6473-6475.

42 L. Tian, D. Ghosh, W. Chen, S. Pradhan, X. J. Chang and S. W. Chen, *Chem. Mater.*, 2009, **21**, 2803-2809.

43 H. Y. Ko, Y. W. Chang, G. Paramasivam, M. S. Jeong, S. J. Cho and S. H. Kim, *Chem. Commun.*, 2013, **49**, 10290-10292.

44 J. Lowy, *Seattle Post-Intelligencer*, 2004.

45 C. Muller, K. Townsend and J. Matschullat, *Science of the Total Environment*, 2012, **416**, 464-467.

46 J. Lapidos, *Slate Magazine*, 2007.

47 B. De and N. Karak, *Rsc Adv.*, 2013, **3**, 8286.

48 P. C. Hsu and H. T. Chang, *Chem. Commun.*, 2012, **48**, 3984-3986.

49 M. Y. Chen, W. Z. Wang and X. P. Wu, *J. Mater. Chem B.*, 2014, **2**, 3937-3945.

50 M. Sevilla and A. B. Fuertes, *Carbon*, 2009, **47**, 2281-2289.

51 X. F. Jia, J. Li and E. K. Wang, *Nanoscale*, 2012, **4**, 5572-5575.

52 R. J. Fan, Q. Sun, L. Zhang, Y. Zhang and A. H. Lu, *Carbon*, 2014, **71**, 87-93.

53 B. D. Wang, J. Hai, Z. C. Liu, Q. Wang, Z. Y. Yang and S. H. Sun, *Angew. Chem., Int. Ed.*, 2010, **49**, 4576-4579.

54 J. A. A. Ho, H. C. Chang and W. T. Su, *Anal. Chem.*, 2012, **84**, 3246-3253.